Metal-insulator-metal diodes with sub-nanometre surface roughness for energy-harvesting applications

Metal-insulator-metal diodes with sub-nanometre surface roughness for energy-harvesting applications

A.A. Khan, G. Jayaswal, F.A. Gahaffar, A. Shamim

PII: S0167-9317(17)30310-6
DOI: doi: 10.1016/j.mee.2017.07.003
Reference: MEE 10620

To appear in: *Microelectronic Engineering*

Received date: 4 April 2017
Revised date: 18 June 2017
Accepted date: 26 July 2017

Please cite this article as: A.A. Khan, G. Jayaswal, F.A. Gahaffar, A. Shamim , Metal-insulator-metal diodes with sub-nanometre surface roughness for energy-harvesting applications, *Microelectronic Engineering* (2017), doi: 10.1016/j.mee.2017.07.003

Metal-Insulator-Metal Diodes with Sub-Nanometre Surface Roughness for Energy-Harvesting Applications

A.A.Khan[!], G.Jayaswal[!], F.A.Gahaffar[!], and A. Shamim[!*]

[!] Electrical Engineering Program, 4700 King Abdullah University of Science and Technology, Thuwal., Saudi Arabia.
*Corresponding author. E-mail: atif.shamim@kaust.edu.sa

***Abstract*— For ambient radio-frequency (RF) energy harvesting, the available power levels are quite low, and it is highly desirable that the rectifying diodes do not consume any power at all. Contrary to semiconducting diodes, a tunnelling diode – also known as a metal-insulator-metal (MIM) diode – can provide zero-bias rectification, provided the two metals have different work functions. This could result in a complete passive rectenna system. Despite great potential, MIM diodes have not been investigated much in the GHz-frequency regime due to challenging nano-fabrication requirements. In this work, we investigate zero-bias MIM diodes for RF energy-harvesting applications. We studied the surface roughness issue for the bottom metal of the MIM diode for various deposition techniques such as sputtering, atomic layer deposition (ALD) and electron-beam (e-beam) evaporation for crystalline metals as well as for an amorphous alloy, namely ZrCuAlNi. A surface roughness of sub-1 nm has been achieved for both the crystalline metals as well as the amorphous alloy, which is vital for the reliable operation of the MIM diode. An MIM diode comprising of a Ti-ZnO-Pt combination yields a zero-bias responsivity of 0.25 V^{-1} and a dynamic resistance of 1200Ω. Complete RF characterisation has been performed by integrating the MIM diode with a coplanar waveguide transmission line. The input impedance varies from 100 Ω to 50 Ω in the frequency range of between 2 GHz and 10 GHz, which can be easily matched to typical antenna impedances in this frequency range. Finally, a rectified DC voltage of 4.7 mV is obtained for an incoming RF power of 0.4 W at zero bias. These preliminary results of zero-bias rectification indicate that complete, passive rectennas (a rectifier and antenna combination) are feasible with further optimisation of MIM devices.**

***Index Terms*— Rectenna, RF-Energy Harvesting, Atomic Force Microscopy (AFM), MIM Tunnelling Diode.**

I. Introduction

Radio-frequency energy harvesting is becoming a popular source of renewable energy for the smart environment, where a large number of sensors and devices are connected to deliver useful information, for example, the Internet of Things (IOT). There is also much interest in powering the systems remotely using far-field RF technology. This is particularly important for many applications, such as small, smart dust sensors [1] or implantable sensors [2]. For remote, wireless powering, a dedicated RF source is used, which can provide sufficient power to operate these sensors, unlike the RF energy-harvesting approach where ambient RF energy is used to power the devices. In the latter case, RF power is low, and thus places many constraints on the efficiency of the system. In both cases, however, a diode is required to rectify the incoming signal from the antenna to obtain a useful DC output.

For energy-harvesting applications, it is highly desirable that the diode does not draw any power for its operation. The process, known as a zero-bias operation [3-4], is typically not feasible with semiconductor-based diodes as they require bias for their operation, and thus consume power. On the other hand, MIM diodes, which work on the principle of electron tunnelling through a thin insulator between the two metals, can be used without being biased as long as metals with different work functions are used [5-6]. For rectification purposes, these diodes can be integrated with an antenna [7] to form a completely passive rectenna system as shown Fig. 1. Their ability to operate under zero-bias conditions and their fast response times as well as the possibility of their realisation through low-cost additive technologies [8] make them attractive for high-frequency applications where typical semiconductor-based devices cannot operate [9].

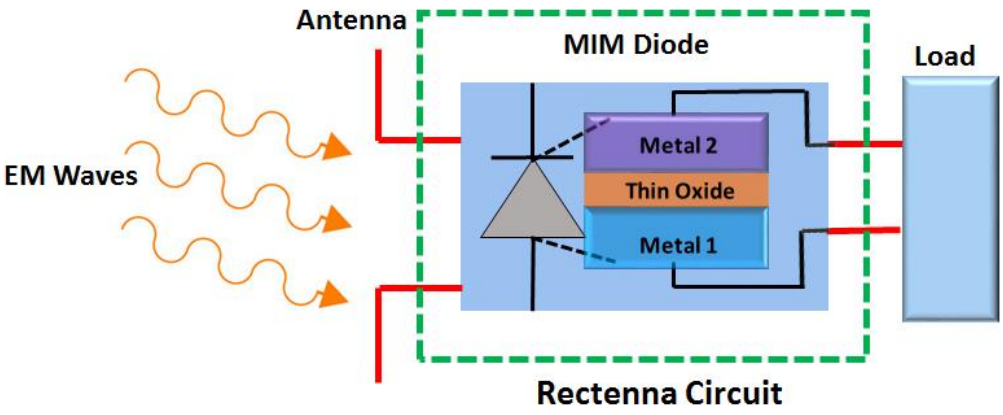

Fig. 1. A schematic of a rectenna device. The frequency received by the antenna is rectified by the MIM diode, which is then further smoothened by the DC filter before being delivered to the load.

Though the real advantage of MIM diodes is high frequencies (THz range), their zero-bias rectification ability can also be beneficial for harvesting and wireless powering at RF frequencies [10]. The trade-off, however, is its poor non-linearity, and subsequently, poor responsivity and rectification ability at present. Moreover, due to the tunnelling operation, it offers high DC resistance. For its realisation, there are two major challenges: firstly, it needs a thin insulator (typically a few nanometres of thin oxide) to ensure electron tunnelling, and secondly, low surface roughness is required, particularly for the bottom metal, to produce reliable and repeatable devices.

Previously reported works on MIM diodes used crystalline metals as the bottom electrodes, without investigating any issues related to the surface roughness of the bottom metal. However, recent work [11] dealt with this issue, and reported that crystalline metals show high surface roughness; therefore, they are not suitable for the bottom electrodes of MIM diodes. That work [11] recommends amorphous alloy films instead of crystalline metals to achieve low surface roughness, but at the cost of much lower conductivities. It is worth mentioning that in [11], the surface-roughness data were collected for different film thicknesses without providing any details on the exact thickness of the films, making it difficult to establish whether the surface roughness is due to the crystalline nature of the metals or because of the thicker crystalline films, as compared to the amorphous alloy films. In this work, we have tried to address this issue, and have provided a detailed comparison between various fabrication methods, crystalline metals and amorphous alloys. This work also presents the achieved surface-roughness values and their effect on the performance of MIM diodes.

Furthermore, most of the work on MIM diodes focuses on high frequencies (THz range) [5-6, 12]. There are only a handful of papers that reported on MIM diodes operating in the RF range, and most of them have serious limitations as far as RF characterisation of the MIM diodes is concerned. In [13], an MIM diode has been measured for its rectification abilities by impinging RF waves directly on the diode using a commercial antenna; however, the major problem is that the diode has not been characterised for its impedance performance using *S*-parameter measurements, which mean that its efficiency cannot be calculated accurately due to the unknown mismatch loss. Furthermore, in the absence of the input impedance of the diode, it is not possible to efficiently integrate it with an RF antenna with appropriate matching. Finally, the authors had operated the diode at non-zero bias voltages, which could result in poor efficiency of the device. Similar works have been reported in [14] and [15], where the authors have provided better RF characterisation of the device. In [14], the diode was characterised for its *S*-parameter measurements using a vector-network analyser (VNA). However, it was never measured for its rectification ability, which is performed by measuring the DC output voltage across a load when the diode is excited by an RF signal. Also, the design that is presented in this work was principally for the THz range of operation; however, due to the lack of measurement equipment at such high frequencies, the authors restricted their characterisation in the GHz range. In [15], the authors characterised the fabricated diode for its input impedance and RF-to-DC conversion abilities. However, the diodes' rectification has been shown with applied bias. From the above literature review, it can be said that both the RF characterisation of an MIM diode and its application at a zero-bias condition still require considerable work and investigation for energy-harvesting applications.

Based on the observations made above, the work presented in this paper reports a systematic study of MIM diodes for RF applications. In addition to the above-mentioned surface-roughness study, we also provide complete DC/RF characterisation. Moreover, RF-to-DC rectification at zero bias is also demonstrated in this work for the first time. In section II, we describe the

operating principle and characteristics of MIM diodes. The investigation of surface roughness for the bottom electrode of MIM diodes, along with the fabrication process and DC response of the diodes, has been summarised in Section III and IV. The RF characterisation of MIM diodes is covered in Section V.

II. METAL-INSULATOR-METAL DIODES

A pn-junction diode can be forward or reverse biased, depending on the polarity of the applied voltage [16]. However, in the absence of any applied voltage, the pn-junction diode will ideally act as an open circuit for any incoming signal. The MIM diode, on the other hand, is a tunnelling device, which is formed by two metal electrodes separated by a thin film of the insulating layer. It works on the principle of quantum-mechanical tunnelling, where electrons tunnel between the two electrodes through an appropriate bias applied across the diode [17]. However, by choosing metals that have different work functions, and by separating them with a suitable insulator, electrons can tunnel without any applied bias [18]. The important parameters for the operation of an MIM diode include the work function of the metals, the electron affinity, the dielectric constant and the physical thickness of the insulator. For our specific MIM diode, the structure is composed of Pt/ZnO/Ti, where Pt has a work function of 5.65 eV and Ti 4.33 eV [19]. The reason for choosing Pt and Ti is to have a higher work-function difference, since a high difference enhances the electron tunnelling [20-21]. The electron affinity of ZnO varies between 2 eV and 2.2 eV, and is taken to be 2.02 eV in our experiment [22-24]. The conduction-band offset diagram is depicted in Fig. 2(a). Fig. 2(b) illustrates the built-in electric field created from the Ti top electrode to the Pt electrode in thermal equilibrium due to the work-function difference between the Ti and Pt electrodes [25]. When a positive voltage is applied to the top electrode, an external field is created from the Ti electrode to the Pt electrode, as demonstrated in Fig. 2(c) [25-27]. The applied electric field causes the electrons to flow from Pt to Ti. When a negative voltage is applied to the Ti top electrode, an external electric field is created from the Pt electrode to the Ti electrode, as illustrated in Fig. 2(d). The flow of current in this direction will be opposite to the case shown in Fig. 2(c). From Fig. 2, it is evident that the difference in the work functions creates a Fermi-level gradient on the both sides of the potential barrier, facilitating electron tunnelling through the oxide layer.

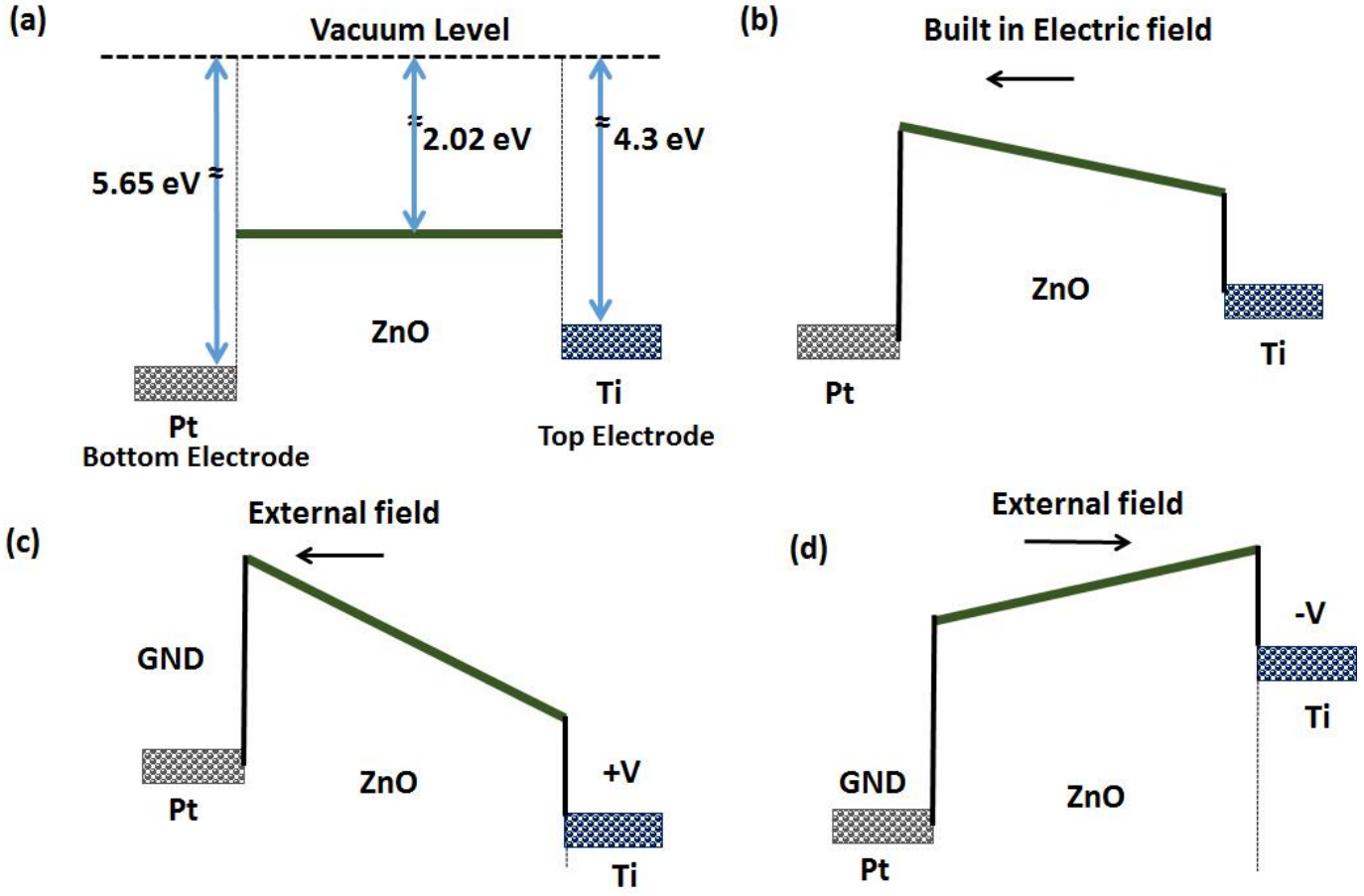

Fig. 2. Energy-band diagram of Pt/ZnO/Ti. (a) Represents the band diagram of Pt/ZnO/Ti. (b) Due to the work function difference between the Pt and Ti electrodes, there is a built-in electric field created from the Ti electrode to the Pt electrode. (c) Under positive bias, external and built-in electric fields are aligned in the same direction. (d) The external and built-in electric fields run in opposite directions under a negative bias.

The probability of electron tunnelling depends on the thickness and the height of the insulator barrier [28]. It is important to compute the number of possibilities that an electron (of given energy) from a metal electrode can tunnel to the empty states of another metal electrode through the insulator. A decrease in the tunnelling distance results in an increase in tunnelling current, and vice versa. However, a physical thickness of the insulator layer is required to isolate the two metal arms. This equates to the non-linear dependence of the tunnelling current on the applied voltage and diode characteristics. Simmons et al. derived a formula for the tunnelling behaviour of electrons through a barrier of any arbitrary shape [28-29]:

$$J = \frac{1.1\,q^2}{4\pi h}\frac{1}{\varphi_b}\left(\frac{V+\Delta\varphi_b}{S}\right)^2 \times \exp\left(\frac{-23\pi\sqrt{qm}}{6h}\varphi_b^{\frac{3}{2}}\left(\frac{S}{V+\Delta\varphi_b}\right)\right) \quad (1)$$

where q is the electric charge, h is Plank's constant, V is the applied bias, φ_b is the barrier height of the electrode-insulator interface from which electrons are tunnelling, $\Delta\varphi_b$ is the difference in barrier heights between the interfaces of the insulator with the top and bottom electrodes (φ_b = the work function of metal-electron affinity of oxide [17, 28]), m is the effective electron mass, S is the tunnel barrier thickness and J is the tunnelling-current density. Based on equation (1), the device will have a non-zero current density even if V is zero, unlike a pn-junction diode. Also, it is evident that the current density decreases with an increase in the tunnel-barrier thickness, and a work-function difference between the two electrodes is required to achieve the tunnelling phenomenon.

The MIM diode's performance is given by three main characteristics: the diode's resistance, responsivity and cut-off frequency. The diode's resistance, commonly known as differential resistance (R_D), is obtained by differentiating current on the applied voltage, which is provided by (2). In general, a low value of R_D is typically required for lower power dissipation from the diode in the on-condition, which is the same for this design. However, another reason for the lower value of R_D is its eventual application in the RF energy-harvesting applications. The diode must be integrated with an RF antenna for collecting the incoming RF waves. Antennae are usually designed to have an impedance of 50 Ω, and higher resistance is detrimental for overall rectenna integration and operation. Therefore, it is important that the diode provides an impedance that is close to antenna impedance to minimise any mismatch losses [5-6, 9, 30].

$$R_D = \frac{1}{I'}, where\ I' = \frac{dI}{dV} \quad (2)$$

The diode's responsivity (R) determines its rectification ability. A higher value of responsivity enhances the AC-to-DC conversion efficiency, and hence increases the rectification ability.

$$R = \frac{I''}{I'}, where\ I'' = \frac{dI^2}{d^2V}\ and\ I = \frac{dI}{dV} \quad (3)$$

The diode's cut-off frequency is given by:

$$f_c = \frac{1}{2\pi R_D C} \quad (4)$$

$$C = \varepsilon_0\varepsilon_{oxide}\frac{A}{d} \quad (5)$$

where R_D is the differential resistance of the diode, C is the diode capacitance, ε_0 and ε_{oxide} are the dielectric constant and relative permeability of oxide, respectively, and A and d are the overlap area and oxide thickness, respectively.

These equations highlight the relationship between device characteristics and material stack, and demonstrate how the choice of material, dielectric constant and chosen thicknesses can all play a significant role in altering MIM-diode characteristics or performance. We have considered all the above aspects in the device design and fabrication.

III. STUDY OF SURFACE ROUGHNESS FOR THE BOTTOM ELECTRODE

As mentioned in the previous section, an MIM diode requires a thin oxide layer (only of few nanometres) that is sandwiched between the two metal electrodes. The current-voltage (IV) characteristics of the diode depend on the tunnelling of the electrons, which can be influenced by both the smoothness and the uniformity of the dielectric layer encapsulated between the two metal electrodes. The surface roughness of this layer is consequently heavily dependent on the bottom metal electrode. Therefore, it is important to study the various factors that can affect the surface roughness of the bottom electrode.

The atomic-scale roughness, along with the non-uniformity of the electrode-insulator interface, could, in the worst-case scenario, cause non-uniform electric fields in the tunnelling region or short circuiting between the two metals. This results in unpredictable device behaviour and low yields [29]. In other words, the lower the surface roughness of the bottom electrode, the higher the yield of the functioning devices. We performed surface-roughness analyses for different metals as well as for an amorphous alloy deposited by various deposition techniques.

The device studied in this experiment is realised on an Si/SiO_2 substrate, where Si (100) is a p-type, Boron-doped wafer with a high resistivity of 550 Ω-cm. First, 300 nm of SiO_2 was thermally grown on the silicon substrate to act as an electrical insulator, and prevent electric-current leakage. Fig. 3. depicts the experimental stack-up used for the surface-roughness study. To enhance the adhesion of the metal, 10 nm of titanium (Ti) was sputtered on top of the SiO_2. Primarily copper (Cu), gold (Au) and platinum (Pt) of different thicknesses were deposited by both sputtering and e-beam evaporation on the adhesion layer to observe the roughness. Additionally, the amorphous alloy, ZrCuAlNi (with an atomic composition of 40% Zr, 35% Cu, 15% Al and 10% Ni), has been studied.

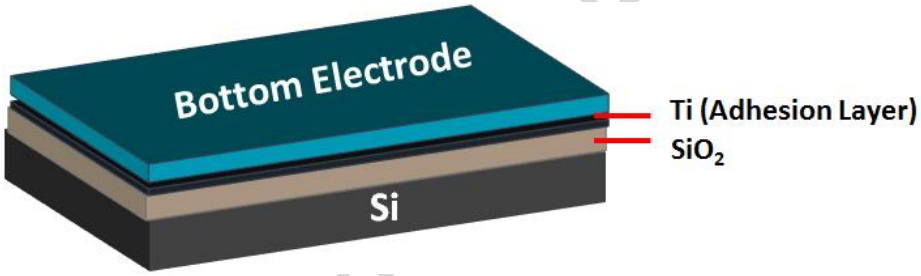

Fig. 3. A schematic demonstration of the stack-up for the surface-roughness study for different metals, which were deposited by various techniques: e-beam evaporation, metal sputtering and ALD.

Atomic-force microscopy (AFM) in contact mode was used to measure the surface profile of metal (Pt) and amorphous alloy (ZrCuAlNi) on an area of 1 x 1 µm2 and 5 x 5 µm2, as illustrated in Fig. 4

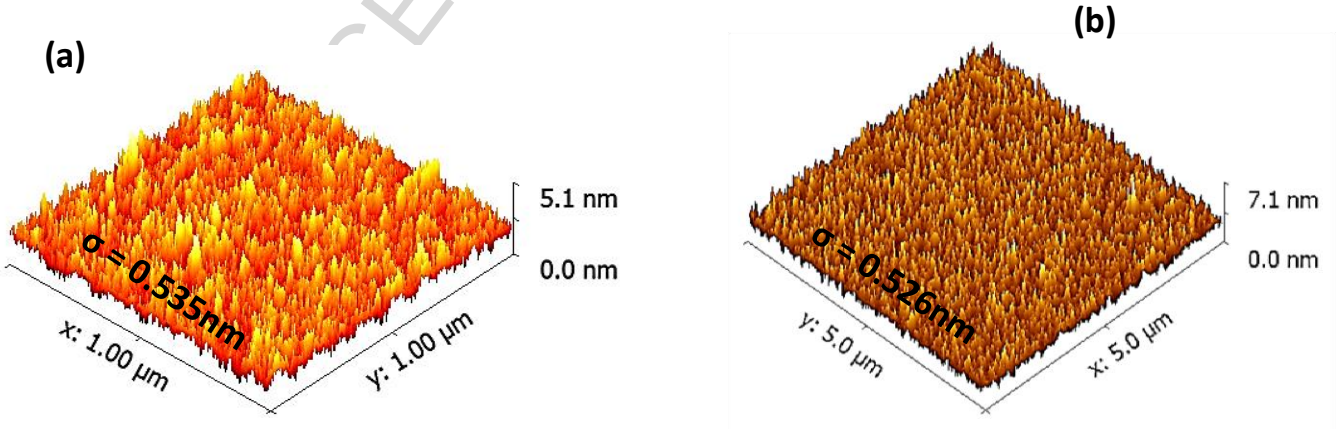

Fig. 4. Measured surface-roughness profile using AFM of (a) Pt with RMS surface roughness = 0.535 nm, and (b) ZrCuAlNi with RMS surface roughness = 0.526 nm.

Table I. summarises the various metals of different thicknesses deposited by the two above-mentioned techniques, namely sputtering and e-beam evaporation. The root mean square (RMS) and peak-roughness values, obtained by AFM, for each sample

are also presented in the table. It can be seen that the thicker metallic layers of Cu and Au (500 nm), deposited by either of the two techniques, display the highest roughness as compared to the films with lower thicknesses (50 nm).

Table I. RMS roughness measured using AFM for crystalline metal and amorphous alloy.

Crystalline metal/Amorphous alloy	**Deposition method**	**Thickness (nm)**	**RMS roughness (σ) (nm)**	**Peak roughness (nm)**
Copper	Sputtering	50	0.58	2.92
Copper	Sputtering	500	2.30	10
Copper	E-Beam Evaporation	50	0.843	3.31
Copper	E-Beam Evaporation	500	1.80	8.29
Platinum	Sputtering	50	0.535	3.61
Gold	Sputtering	500	2.65	12.8
ZrCuAlNi	Sputtering	50	0.526	2.69

Based on the AFM study, it can be observed that with a lower thickness (50 nm), a sub-1 nm roughness for crystalline metals deposited by sputtering and e-beam evaporation can be achieved. Furthermore, sputtered Cu and Pt with 50 nm thicknesses show the least surface roughness, which is comparable to the values obtained for ZrCuAlNi amorphous alloy. This is in contrast to the previous study [11] in which it was concluded that crystalline metals could not achieve the same lower surface roughness as that of an amorphous alloy. Note that in this study, we used the same amorphous alloy as has been used by ref [11], so that a fair comparison can be done. This is a significant finding because amorphous alloys have poor conductivity, and thus cannot be used in place of high-conductivity metals.

IV. MIM DIODE FABRICATION AND CHARACTERISATION

After assessing the proper technique for bottom-metal deposition to yield minimal surface roughness, the fabrication of a complete MIM diode was undertaken. As depicted in the schematic of Fig. 5, the device was realised on a standard Si/SiO_2 substrate (Fig. 5(a)). The first (or bottom) electrode of the MIM diode was fabricated using a sputtered Pt film and lift-off process for smooth metal deposition and device patterning. To do so, a photoresist (ECI-5214) with a thickness of ~ 1.6 µm was spin-coated on the top surface of Si/SiO_2 to act as a photosensitive polymer and pattern exposure (Fig. 5(b)). Then, the bottom arm was patterned using UV lithography. After the UV exposure (dose 80 mJ/cm^2), the pattern was developed in a solution of MIF-926 (Fig. 5(c)). After development, O_2 descum was used for 30 seconds to remove the residual photoresist. Then, 10 nm/50 nm Ti/Pt was deposited using sputtering (Fig. 5(d)). Since Pt is known to have poor stiction to SiO_2 films, we sputtered a thin layer of Ti as an adhesion layer. Finally, patterning was done through a lift-off process by sonicating our sample in acetone for 5 minutes (Fig. 5(e)).

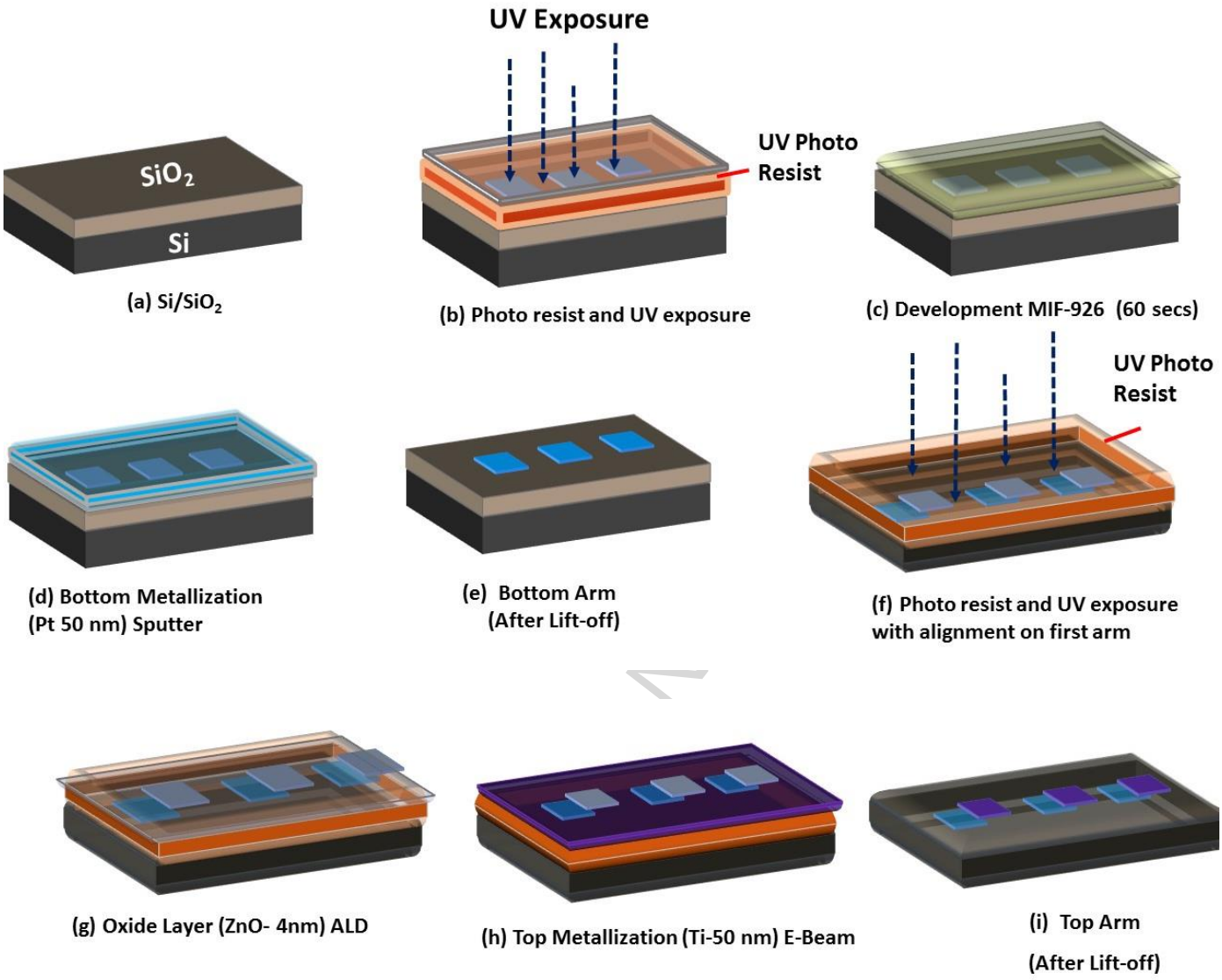

Fig. 5. Fabrication of an MIM device. a) Si/SiO2. b) First arm exposure by UV lithography. c) Removing the exposed resist using an MIF-926 developer. d) First arm sputtering of Ti/Pt. e) First arm after lift-off. f) Second arm alignment, and exposure by UV lithography. g) Oxide-layer deposition after resist development. h) Top arm (Ti 50 nm) e-beam. i) Final MIM device after lift-off.

Next is the deposition of the thin (4 nm) ZnO (Fig. 5(g)). This was done using ALD to ensure uniform and conformal deposition. Then, to overlap the second (or top) arm, we deposited Ti metal using an e-beam evaporation technique, and patterning using lift-off. To realise this controlled overlap, an alignment procedure was carried out by using precise alignment marks during the UV lithography process (Fig. 5(f)). Using the same previously mentioned parameter for UV exposure, the pattern resist was again developed. Then we proceeded by depositing 50 nm of Ti using e-beam evaporation (Fig. 5(h)), instead of traditional sputtering, to prevent surface damage of the oxide from plasma and ion bombardment. The patterning of the Ti metal was again performed through a lift-off process by sonicating the sample in acetone for 5 minutes (Fig. 5(i)).

Finally, to facilitate and enable RF measurements for our MIM diode structure, it was necessary to deposit separate measuring pads, which were aligned and patterned by UV exposure using the same parameters as mentioned above. To do so, Cu with a thickness of 500 nm was sputtered to form the RF contact pads. The optical image of the MIM diode is illustrated in Fig. 6, where the tunnelling diode is obtained at the overlap junction of the two dissimilar metals (Pt and Ti); the metal arms having different work functions.

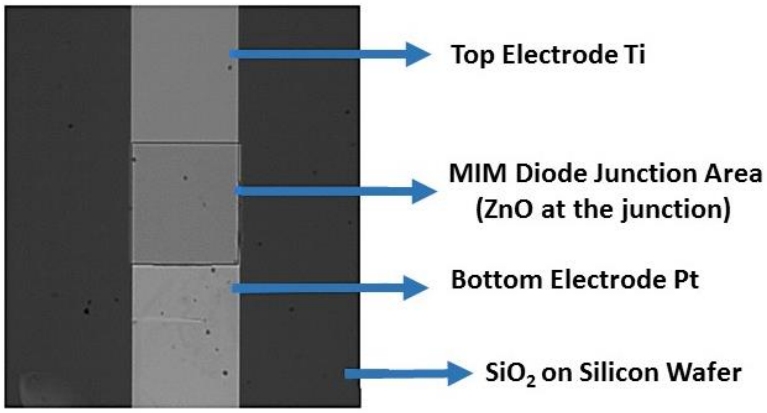

Fig. 6. An optical microscopic image of a fabricated MIM diode (Pt/ZnO/Ti) with an overlap area of 0.09 mm^2, where the tunnelling diode is sandwiched between two dissimilar metals.

To view the material composition of the fabricated device (Pt/ZnO/Ti), a cross-section image was obtained using TEM (Titan 80-300 ST), as demonstrated in Fig. 7(a). To image the thickness of a few nanometres of a ZnO layer, a highly focused and magnified electron beam was used near the metal/oxide junction. An Energy-Dispersive X-Ray (EDX) analysis was also performed on the fabricated device for the elemental analysis. The TEM images in Fig. 7(a) highlight our optimised process steps with smooth surface roughness for our bottom Pt electrode and top Ti metal layer. It is evident from Fig. 7(b) that the number of counts obtained during the EDX analysis corresponds to the material stack-up used in our fabrication.

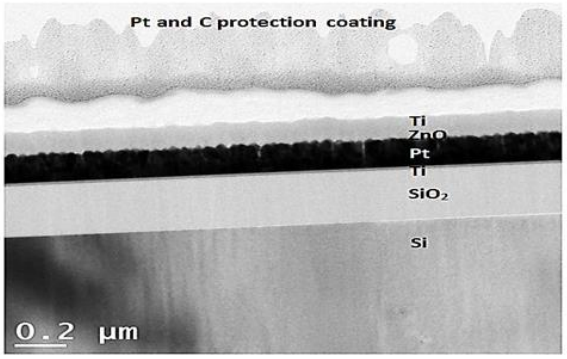

Fig. 7 (a). Cross-sectional TEM (dark field) image of the fabricated diode. The diagram showing the individual material stack-up of the device Si/SiO2/Ti/Pt/ZnO/Ti stack up.

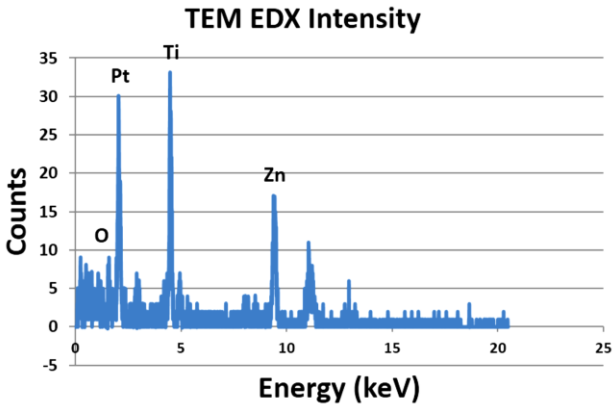

Fig. 7 (b). TEM EDX spectrum of the fabricated diode. Analysis at ZnO insulator interface indicated the presence of Zn and O peak. The analysis also confirms the presence of Pt and Ti in the fabricated diode.

IV.2. DC CHARACTERISATION

We then proceed with electrical characterisation (I-V) to assess the responsivity and the differential resistance of our fabricated Pt/ZnO/Ti MIM diodes. The DC characteristics were extracted using a four-point probe method and a Keithley semiconductor parametric analyser. To prevent any damage to the devices, voltage sweep from -1 V to +1 V was restricted. The two main performance parameters i.e. dynamic resistance and responsivity were extracted from the I-V measurements using equations (2) and (3). To reduce the effects of noise, the diodes' I-V curves were smoothened and fitted with a fourth-order polynomial before calculating the resistance and responsivity. As mentioned previously, for energy-harvesting applications, it is important for the diodes to operate at zero bias. Therefore, we focused on calculating the zero-bias resistance (R_D) and zero-bias responsivity (R). The result for one of the diodes is presented in Fig. 8, which indicates an $R_D \sim 1210\ \Omega$ (Fig. 8(a)) and an R of $0.25V^{-1}$ (Fig. 8 (b)). Comparison with the literature shows that the zero-bias resistance is in the reasonable range. Apart from a

few cases in which a zero-bias resistance of less than 500 Ω was reported [7, 12, 31], it has mostly been in the range of *M* Ω [32-35]. Though the zero-bias responsivity is relatively low, it is consistent with the lower zero-bias resistance values. As typically demonstrated [36], higher responsivity can be achieved at the expense of higher resistance (~ *M* Ω); however, this is detrimental to overall rectenna integration and operation.

Moreover, the non-zero responsivity at zero bias demonstrates the rectification ability of our device, and hence it can be used for energy-harvesting applications without any aid of external bias.

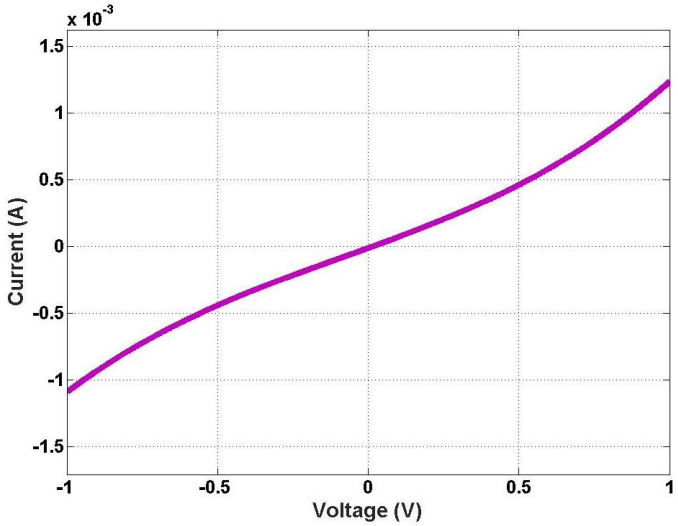

(a)

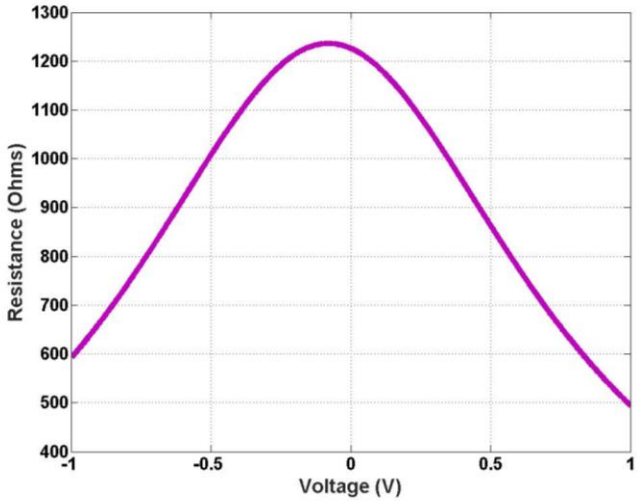

(b)

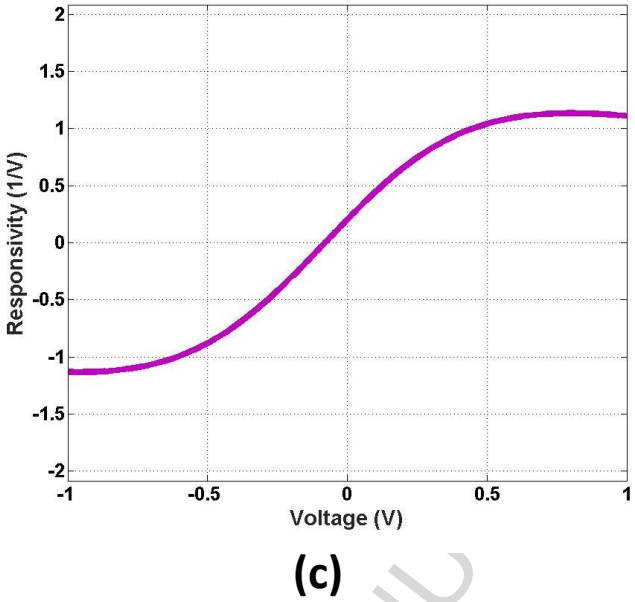

(c)

Fig. 8. The I-V characteristics, resistance and responsivity of the fabricated Pt/ZnO/Ti MIM diode using a four-probe measurement. (a) Measured diode DC I-V characteristic. (b) Measured resistance. (c) Measured responsivity. The zero-bias resistance and responsivity is estimated to be 1210 Ω and $25V^{-1}$ respectively.

V. RADIO-FREQUENCY CHARACTERISATION OF MIM DIODES

An important aspect of this work is the comprehensive RF characterisation of MIM diodes. High-frequency characterisation is crucial to demonstrate the ability of these devices for rectifier applications. The DC characterisation of the fabricated MIM diodes demonstrated a zero-bias responsivity of 0.25 V^{-1}. A non-zero responsivity value shows that the diodes can be used for rectification without using any DC bias. To study the RF behaviour of the diode, it is first characterised for its S- parameters. This measurement is used to extract the input impedance of the diode. Thereafter, the diode is connected to an RC load, and excited with an RF signal. The DC power measured across the load versus the applied RF signal's power determines the rectification ability of the device.

(a)

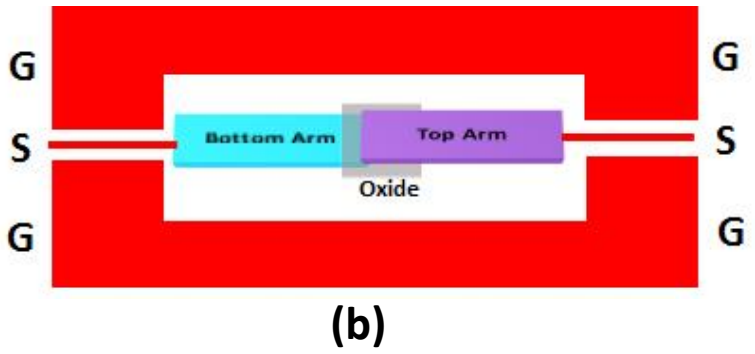

Fig. 9. The MIM diode integrated with a coplanar waveguide (CPW) – Ground-Signal-Ground (G-S-G) – used for *S*-parameter measurements. (a) The CPW with line width = 0.1 mm with a gap of 0.06 mm. (b) The MIM diode integrated with CPW.

A. Radio Frequency Characterisation using S-parameters and Input Impedance of the MIM Diode:

As a first step, the diode is measured for its *S*-parameters. The diode is a two-terminal device that can be easily tested for its IV curve using the DC probes. However, for RF characterisation, it is important that the diode is integrated with a transmission line for proper RF mode propagation. Therefore, the diode is integrated with a CPW structure to measure its *S*-parameters, as illustrated in Fig. 9. The CPW has been designed to have a characteristic impedance (Z_0) of 50 Ω.

Keysight's Performance Network Analyser (PNA) is used for *S*-parameter measurements, and RF probes with a pitch size of 150 µm are used for signal excitation. Short-Open-Load-Through (SOLT) calibration has been performed from 0.5 GHz to 10 GHz on an SOS Microtec, CSR-4 Impedance Standard Substrate (ISS). Once calibrated, the MIM diode with a CPW feed can be measured for its *S*-parameters. The measured results for the transmission and reflection coefficients of the diode are shown in Fig. 10 (a). As expected, the S_{11} and S_{22} parameters (representing mismatch and reflection at the input and output ports, respectively) are quite high. This means that a considerable amount of power is reflected back. However, this behaviour is typical of a diode before matching. It is important to clarify here that the diode's *S*-parameters are expected to show a mismatch, since it is intentionally not matched to the PNA's 50 Ω impedance in order to study the input impedance of the diode. The study of the diode's input impedance versus frequency is essential to integrate it with the antenna; the antenna and diode impedances must be matched to the frequency of interest to avoid a mismatch loss. This requires the designer to know the actual input impedance of the two components. According to [37] the S-parameters can be expressed in terms of impedance or *Z*-parameters as they are interchangeable. Herein, the input impedance of the diode is extracted from the Z-parameters (calculated from *S*-parameters) using (equation 7) and is shown in Fig. 10 (b).

$$Z_{in} = Z_{11} - \frac{(Z_{12}.Z_{21})}{Z_{22}+Z_0}, where\ Z_0 = 50\,\Omega \qquad [7]$$

From the input-impedance plot, it can be observed that for the lower frequency band, the diode exhibits high values for the actual impedance (300 Ω to 400 Ω), while for higher frequencies, the value decreases to 10 s of ohm. For the imaginary impedance, the diode's capacitive behaviour, which is the usual response of an MIM structure, is evident. Nevertheless, it can be seen that the actual component of the input impedance varies from 100 Ω to 50 Ω in the frequency range of 2 GHz to 10 GHz, and the imaginary components are quite small. Therefore, in this frequency range, the diode's input impedance can be matched to the typical 50 Ω or 100 Ω antenna impedance.

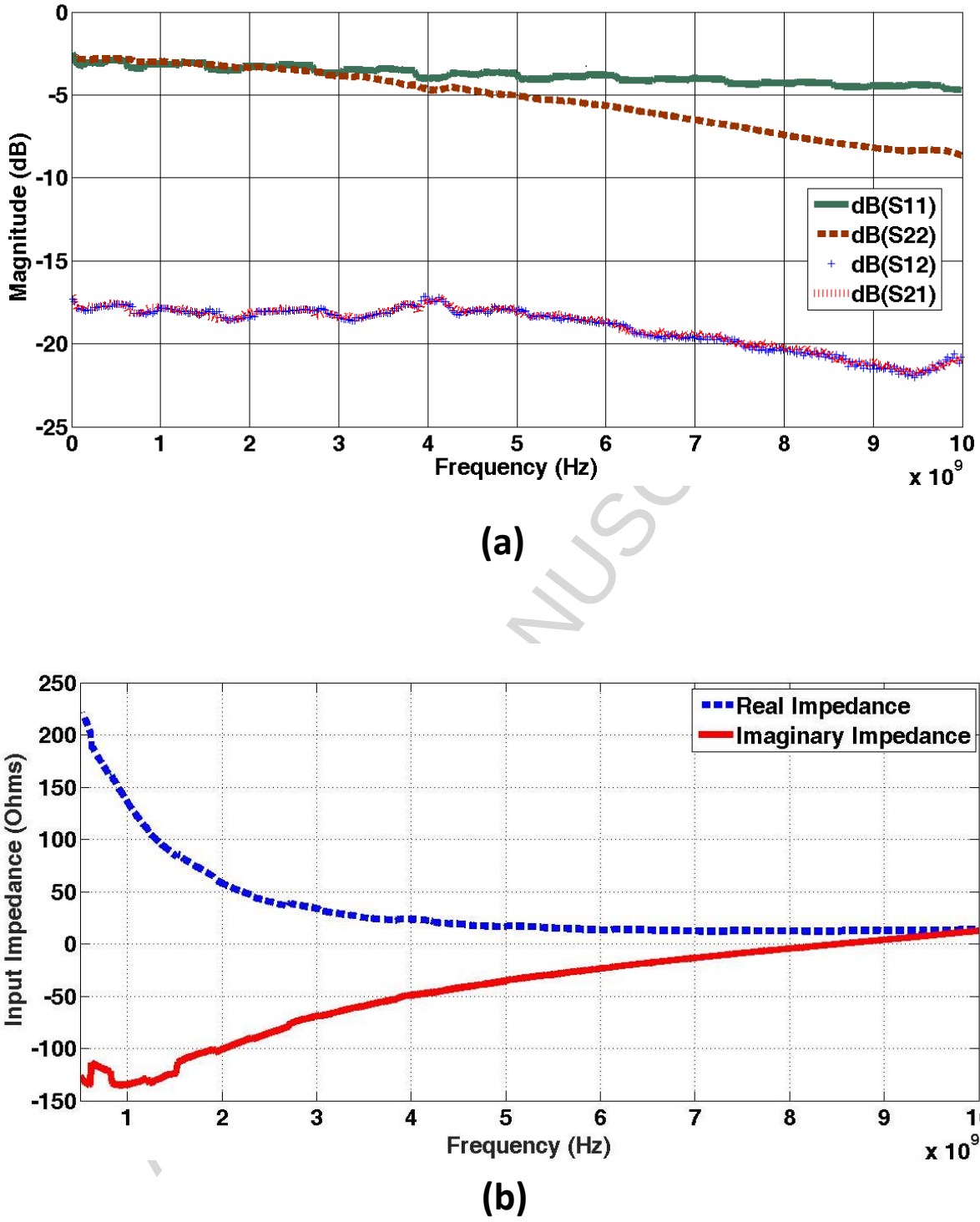

Fig. 10. Measured *S*-parameters and input impedance of the fabricated device. (a) two port *S*-parameters showing transmission and reflection parameters for both the ports, (b) Real and Imaginary parts of the input impedance of the diode which have been extracted from the measured *S*-parameters.

B. Radio Frequency Characterisation using RF-to-DC rectification with an MIM Diode:

To verify the suitability of this diode for the rectifier circuit, the diode needs to be tested for its RF-to-DC conversion abilities. This is done by attaching a suitable load to the diode and measuring the DC voltage across this load for varying input RF power.

The set-up for this experiment is illustrated in Fig. 11 (a), and the actual device during RF characterisation is depicted in Fig. 11 (b). The frequency of operation for this measurement is 2.45 GHz, while power to the input of the diode is swept from 0 W to 0.7 W. A resistor of 100 kΩ and capacitor of 100 pF are used as the loads to the rectifying diode.

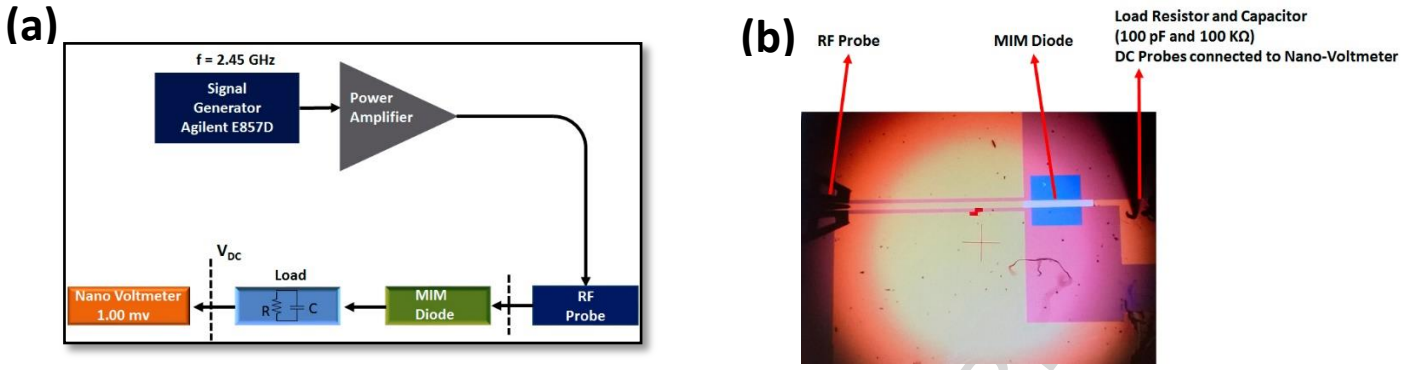

Fig. 11. (a) A block diagram showing RF-to-DC rectification-measurement set-up for MIM diodes. (b) A microscopic image showing RF-characterisation set-up, wherein the MIM diode, load area and RF probe are clearly visualised.

Radio-frequency power is excited at the input of the diode through a power amplifier, while DC voltage is measured across the load using Keithley's nano-voltmeter – these measurements are done without applying any bias across the diode, maintaining the zero-bias operation.

The DC voltage, measured at the load versus the input-RF power, is shown in Fig. 12. A maximum voltage of 4.7 mV is obtained for an RF power 0.4 W. Beyond this point, the amplifier used at the output of the signal generator seems to be saturated, and provides a constant output power. Therefore, no increment in DC voltage is observed. It is worth mentioning here that the mismatch at the diode input has been taken into account for these measurements.

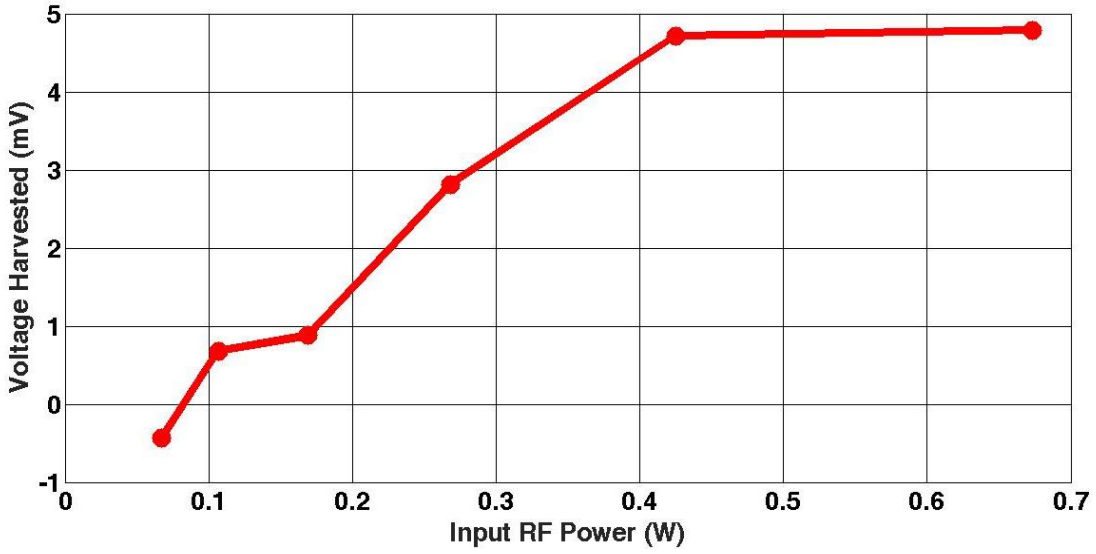

Fig. 12. Graph showing voltage harvested from input RF power for the fabricated MIM diode at 2.45 GHz frequency.

Although this DC-voltage value is small, it must be considered that the MIM diode device used here has a small area of 0.01 mm^2. Also, its non-linearity, and subsequently the rectification ability, is not the best, and can be further optimised. It is expected that, with optimisation of the device structure, for example, using different insulator layers (which are expected to enhance the non-linearity), the output DC voltage can be increased. Nonetheless, it is encouraging to see that at zero bias, rectification of the RF signals is possible. As per the authors' knowledge, this is the first demonstration of rectification of an RF signal using an

MIM diode at zero bias. This demonstrates the potential of using an MIM diode as a rectifier in RF applications, such as passive rectenna design.

VI. CONCLUSION

In this work, MIM diodes were investigated for RF energy-harvesting applications. The issue of surface roughness for the bottom electrode of an MIM diode was studied for both crystalline metals as well as an amorphous alloy. This study was conducted through AFM for crystalline metals as well as an amorphous alloy that were deposited using various techniques such as ALD, e-beam evaporation and sputtering. Additionally, surface-roughness analysis has been performed for an amorphous alloy to compare its results with those of crystalline metals. It is concluded that a sub-1 nm surface roughness can be achieved for crystalline metals, and is comparable to the surface roughness achieved for the amorphous alloy through a traditional deposition method, namely sputtering. In the second part of the study, complete MIM diodes were fabricated using Pt metal as the bottom electrode, deposited through the sputtering process. DC characterisation indicated that the MIM diode could provide a zero-bias responsivity of 0.25 V^{-1} with a decent dynamic resistance of 1200 Ω. Metal-Insulator-Metal diode RF characterisation was done using two methods: 1) *S*-parameter measurements from 500 MHz to 10 GHz, and 2) RF-to-DC rectification at zero bias. The presented results of input impedance can be useful for the integration of MIM diodes with antennae for harvesting applications. The second part of RF characterisation verified the zero-bias RF-to-DC rectification.

VII. ACKNOWLEDGEMENT

We acknowledge financial support from the King Abdullah University of Science and Technology (KAUST) and the Office of Sponsored Research (OSR) for CRG grant OCRF-2014-CRG-62140381. The authors would also like to thank Nini Wei and Anjum Dalaver for their help with TEM analysis.

REFERENCES

[1] T. Salter, G. Metze, and N. Goldsman, "Parasitic aware optimization of an RF power scavenging circuit with applications to Smartdust sensor networks," in Radio and Wireless Symposium, 2009. RWS'09. IEEE, pp. 332-335, 2009.

[2] S. Ladan and K. Wu, "High efficiency low-power microwave rectifier for wireless energy harvesting," in Microwave Symposium Digest (IMS), 2013 IEEE MTT-S International, pp. 1-4, 2013.

[3] Fumeaux, C., W. Herrmann, F. K. Kneubühl, and H. Rothuizen. "Nanometer thin-film Ni–NiO–Ni diodes for detection and mixing of 30 THz radiation." Infrared physics & technology 39, no. 3: 123-183, 1998.

[4] S. Grover and G. Moddel, "Metal Single-Insulator and Multi-Insulator Diodes for Rectenna Solar Cells," in Rectenna Solar Cells, ed: Springer, pp. 89-109, 2013.

[5] Joshi, Saumil, and Garret Moddel. "Simple Figure of Merit for Diodes in Optical Rectennas." IEEE Journal of Photovoltaics 6, no. 3: 668-672, 2016.

[6] Gadalla, M. N., M. Abdel-Rahman, and Atif Shamim. "Design, optimization and fabrication of a 28.3 THz nano-rectenna for infrared detection and rectification." Scientific reports 4, 2014.

[7] M. Abdel-Rahman, F. Gonzalez, and G. Boreman, "Antenna-coupled metal-oxide-metal diodes for dual-band detection at 92.5 GHz and 28 THz," Electronics Letters, vol. 40, pp. 116-118, 2004.

[8] M. Bareiss, et al. "Nano-transfer printing of functioning MIM tunnel diodes." Silicon Nanoelectronics Workshop (SNW), 2012 IEEE. IEEE, 2012.

[9] Grover, Sachit, and Garret Moddel. "Applicability of metal/insulator/metal (MIM) diodes to solar rectennas." IEEE journal of photovoltaics 1, no. 1: 78-83, 2011.

[10] K. Choi, F. Yesilkoy, G. Ryu, S. H. Cho, N. Goldsman, M. Dagenais, and M. Peckerar, "A focused asymmetric metal–insulator–metal tunneling diode: fabrication, DC characteristics and RF rectification analysis," Electron Devices, IEEE Transactions on, vol. 58, pp. 3519-3528, 2011.

[11] N. Alimardani, "Investigation of metal-insulator-metal (MIM) and nanolaminate barrier MIIM tunnel devices fabricated via atomic layer deposition," Ph.D. dissertation, Oregon State University, 2013.

[12] I. Wilke, Y. Oppliger, W. Herrmann, and F. Kneubühl, "Nanometer thin-film Ni-NiO-Ni diodes for 30 THz radiation," Applied Physics A, vol. 58, pp. 329-341, 1994.

[13] K. Choi, F. Yesilkoy, G. Ryu, S. H. Cho, N. Goldsman, M. Dagenais, and M. Peckerar, "A focused asymmetric metal–insulator–metal tunneling diode: fabrication, DC characteristics and RF rectification analysis," Electron Devices, IEEE Transactions on, vol. 58, pp. 3519-3528, 2011.

[14] O. A. Ajayi, "DC and RF Characterization of High Frequency ALD Enhanced Nanostructured Metal-Insulator-Metal Diodes," 2014.

[15] A. Kaur, X. Yang, and P. Chahal, "Study of microwave circuits based on Metal-Insulator-Metal (MIM) diodes on flex substrates," in Electronic Components and Technology Conference (ECTC), 2014 IEEE 64th, pp. 2168-2174, 2014.

[16] Streetman, B. G., & Banerjee, S. (2000). Solid state electronic devices (Vol. 4, p. 89). New Jersey: Prentice Hall.

[17] Moddel, Garret, and Sachit Grover, eds. Rectenna solar cells. Vol. 4. New York: Springer, 2013.

[18] J. A. Bean, A. Weeks, and G. D. Boreman, "Performance optimization of antenna-coupled Al/AlOx/Pt tunnel diode infrared detectors," IEEE J. Quantum Electron, vol. 47, pp. 126-135, 2011.

[19] Palik, E. D. (1998). Handbook of optical constants of solids (Vol. 3). Academic press.

[20] Periasamy, P., Berry, J. J., Dameron, A. A., Bergeson, J. D., Ginley, D. S., O'Hayre, R. P., & Parilla, P. A. (2011). Fabrication and characterization of MIM diodes based on Nb/Nb2O5 via a rapid screening technique. Advanced Materials, 23(27), 3080-3085, 2011.

[21] Periasamy, P., Guthrey, H.L., Abdulagatov, A.I., Ndione, P.F., Berry, J.J., Ginley, D.S., George, S.M., Parilla, P.A. and O'Hayre, R.P. Metal–insulator–metal diodes: Role of the insulator layer on the rectification performance. Advanced Materials, 25(9), pp.1301-1308, 2013.

[22] D. C. Look, "Recent advances in ZnO materials and devices," Materials Science and Engineering: B, vol. 80, pp. 383-387, 2001.

[23] J. H. Kim, X. Li, L.-S. Wang, H. L. de Clercq, C. A. Fancher, O. C. Thomas, and K. H. Bowen, "Vibrationally resolved photoelectron spectroscopy of MgO-and ZnO-and the low-lying electronic states of MgO, MgO-, and ZnO," The Journal of Physical Chemistry A, vol. 105, pp. 5709-5718, 2001.

[24] T. Hanada, "Basic Properties of ZnO, GaN, and Related Materials," in Oxide and Nitride Semiconductors, ed: Springer, pp. 1-19, 2009.

[25] F.-C. Chiu, "A review on conduction mechanisms in dielectric films,
"Advances in Materials Science and Engineering, vol. 2014, 2014.

[26] J. Robertson, "Band offsets of wide-band-gap oxides and implications for future electronic devices," Journal of Vacuum Science & Technology B, vol. 18, pp. 1785-1791, 2000.

[27] Cowell III, E. W., Muir, S. W., Keszler, D. A., & Wager, J. F. (2013). Barrier height estimation of asymmetric metal-insulator-metal tunneling diodes. Journal of Applied Physics, 114(21), 213703, 2013.

[28] J. G. Simmons, "Generalized formula for the electric tunnel effect between similar electrodes separated by a thin insulating film," Journal of Applied Physics, vol. 34, pp. 1793-1803, 1963.

[29] N. Alimardani, E. W. Cowell III, J. F. Wager, J. F. Conley Jr, D. R. Evans, M. Chin, S. J. Kilpatrick, and M. Dubey, "Impact of electrode roughness on metal-insulator-metal tunnel diodes with atomic layer deposited Al2O3 tunnel barriers," Journal of Vacuum Science & Technology A, vol. 30, p. 01A113, 2012.

[30] Wang, K., Hu, H., Lu, S., Guo, L., Zhang, T., Han, Y., Zhou, A. and He, T., 2016. Design and analysis of a square spiral nano-rectenna for infrared energy harvest and conversion. Optical Materials Express, 6(12), pp.3977-3991, 2016.

[31] A. Kaur, X. Yang, and P. Chahal, "Study of microwave circuits based on Metal-Insulator-Metal (MIM) diodes on flex substrates," in Electronic Components and Technology Conference (ECTC), 2014 IEEE 64th, 2014, pp. 2168-2174, 2014.

[32] S. Krishnan, H. La Rosa, E. Stefanakos, S. Bhansali, and K. Buckle, "Design and development of batch fabricatable metal–insulator–metal diode and microstrip slot antenna as rectenna elements," Sensors and Actuators A: Physical, vol. 142, pp. 40-47, 2008.
[33] J. A. Bean, A. Weeks, and G. D. Boreman, "Performance optimization of antenna-coupled Al/AlOx/Pt tunnel diode infrared detectors," IEEE J. Quantum Electron, vol. 47, pp. 126-135, 2011.
[34] S. Zhang, L. Wang, C. Xu, D. Li, L. Chen, and D. Yang, "Fabrication of Ni-NiO-Cu Metal-Insulator-Metal Tunnel Diodes via Anodic Aluminum Oxide Templates," ECS Solid State Letters, vol. 2, pp. Q1-Q4, 2013.
[35] M. Abdel-Rahman, M. Syaryadhi, and N. Debbar, "Fabrication and characterisation of high sensitivity copper-copper oxide-copper (Cu-CuO-Cu) metal-insulator-metal tunnel junctions," Electronics Letters, vol. 49, pp. 363-364, 2013.
[36] A. Hoofring, V. Kapoor, and W. Krawczonek, "Submicron nickel-oxide-gold tunnel diode detectors for rectennas," Journal of Applied Physics, vol. 66, pp. 430-437, 1989.
[37] Pozar, David M. Microwave engineering. John Wiley & Sons, 2009 (chapter-4).

Graphical abstract

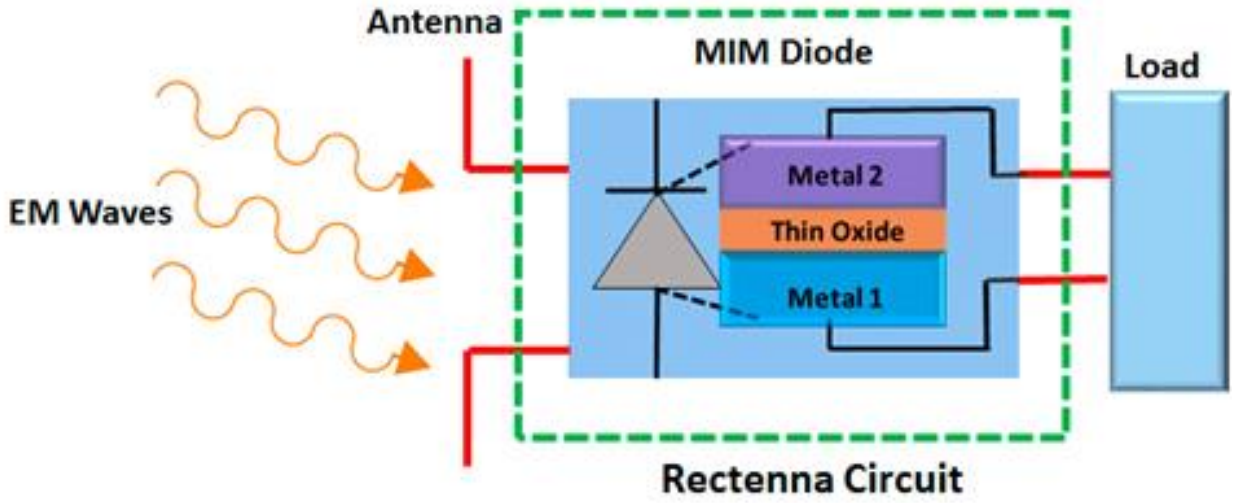

Highlights

- A novel and systematic study of Metal Insulator Metal Diode (MIM) for Radio Frequency (RF) applications.
- Study of the surface roughness for the bottom electrode of MIM diode deposited by various deposition techniques.
- Important conclusion is that a sub-nm surface roughness can be achieved for crystalline metals as well as for an amorphous alloy (ZrCuAlNi).
- Complete DC and RF characterization results are presented, indicating a decent responsivity at zero-bias.
- Successful demonstration of the rectification of an RF signal using MIM diode at zero bias, which is an important step towards completely passive rectennas.